Backward running or absence of running from Creutz ratios

Joel Giedt* and Evan Weinberg†

Department of Physics, Applied Physics and Astronomy,

Rensselaer Polytechnic Institute, 110 8th Street, Troy NY 12065 USA

(Dated: Aug. 19, 2011)

Abstract

We extract the running coupling based on Creutz ratios in SU(2) lattice gauge theory with two Dirac fermions in the adjoint representation. Depending on how the extrapolation to zero fermion mass is performed, either backward running or an absence of running is observed at strong bare coupling. This behavior is consistent with other findings which indicate that this theory has an infrared fixed point.

PACS numbers: 11.10.Hi,11.15.Ha,12.60.Nz

---

*Electronic address: giedtj@rpi.edu

†Electronic address: weinbe2@rpi.edu

I. MOTIVATION

Understanding the allowed model space in extensions to Standard Model is a research program that gains motivation at the onset of the Large Hadron Collider. In technicolor models, the Higgs mechanism occurs through condensation of new fermions that are subject to a gauge interaction that is strong at the TeV scale [1, 2]. Walking technicolor is a version of this theory that can address certain difficulties associated with flavor-changing neutral currents [3–9]. Higher representations of the gauge group are believed to avoid problems with the S-parameter, i.e. electroweak precision constraints [10, 11]. All of this has motivated the study of Minimal Walking Technicolor [12] using lattice techniques, in order to see where this theory lies with respect to the conformal window. In other words, there is no guarantee that the theory actually walks; finding out one way or another is to solve a strong coupling problem. Here we discuss a method, based on the behavior of Creutz ratios, that does just that. The approach taken here is different from the Schrödinger functional method that was employed for SU(3) gauge group with triplet fermions in [13], SU(3) gauge group with sextet fermions [14], and Minimal Walking Technicolor [15–17]. The latter works indicate the existence of an infrared fixed point. We obtain results consistent with that conclusion by this alternate Creutz ratio approach.

II. THE METHOD

In [18] a method for measuring the running gauge coupling on the lattice using Creutz ratios was proposed. In [19, 20] this method was applied to pure SU(3) lattice Yang-Mills, and in [20, 21] this method was applied in a preliminary way to SU(3) gauge group with sixteen triplet fermions, and more recently in [22] to SU(2) gauge group with eight flavors of fundamental representation fermions. We will use this approach to search for the phenomenon of backward running, which is a smoking gun for a nontrivial infrared fixed point, since forward running is assured at weak coupling by perturbative methods. We apply the method of Creutz ratios to the theory of Minimal Walking Technicolor: SU(2) gauge theory with two flavors of fermions in the adjoint representation. Our lattice action is Wilson fermions and a plaquette gauge action.

A. Outline

The proposal [18] defines the running coupling $g(L)$ at a scale $L = Na$ associated with the spatial extent of the lattice, where N is the number of sites in spatial directions and a is the lattice spacing.[1] This is done through the Creutz ratio [23]:

$$\chi(I,J) = -\ln \frac{W(I,J)W(I-1,J-1)}{W(I,J-1)W(I-1,J)} \tag{2.1}$$

where $W(I,J)$ is the expectation value of the trace of the rectangular $I \times J$ Wilson loop on the lattice. Throughout, we only consider $\chi(I,I)$. The Creutz ratio is interpolated between values of I to define a related function $\tilde{\chi}(\hat{R})$ with $\hat{R} \equiv R/a$ continuous. The interpolation requires a matching of values at the points where $\hat{R}$ is half-integral:

$$\tilde{\chi}(\hat{R}) \equiv \chi(\hat{R}+\frac{1}{2}, \hat{R}+\frac{1}{2}) = -\ln \frac{W(\hat{R}+\frac{1}{2},\hat{R}+\frac{1}{2})W(\hat{R}-\frac{1}{2},\hat{R}-\frac{1}{2})}{W(\hat{R}+\frac{1}{2},\hat{R}-\frac{1}{2})^2} \tag{2.2}$$

the logic being that the Wilson loops appearing in the Creutz ratio have average size R. In fact, taking the classical continuum limit, one finds that the Creutz ratio is a finite difference approximation:

$$\hat{R}^2\tilde{\chi}(\hat{R}) \approx -RT\frac{\partial^2}{\partial R \partial T} \ln W_{\text{cont.}}(R,T)\bigg|_{T=R}, \tag{2.3}$$

where $W_{\text{cont.}}(R,T) \approx W(\hat{R},\hat{T})$ is the Wilson loop in the continuum language. T here should not be confused the temporal extent of the lattice.

In the Creutz ratio method for determining $g(L)$, we choose

$$r = R/L = \text{fixed}. \tag{2.4}$$

Note also that we have to deal with a fermion mass m_q, which we take to be the PCAC mass. Our approach will be to measure $g(L)$ at nonzero m_q and then extrapolate to the $m_q = 0$ limit.

The important thing that Bilgici et al. have noted is that at one loop in lattice perturbation theory, including the effect of bosonic zero modes,

$$\hat{R}^2\tilde{\chi}_{\text{1-loop}}(L,a|\hat{R}) = k(r,N)g_0^2, \quad N = L/a \tag{2.5}$$

---

[1] In our analysis we take temporal extent $T = 2L$, to allow for accurate measurement of the partially conserved axial current (PCAC) mass and reuse of the lattice configurations for studies of the spectrum. In fact, this is an advantage of the Creutz ratio method over Schrödinger functional studies.

which defines the quantity $k(r,N)$. Here, g_0 is the bare coupling. It was found in [18, 19] that in the limit of large N, $k(r,N) \to k(r)$, so that it is an L and a independent quantity in the continuum limit. Thus we write $k(r)$ in what follows, and will define the running coupling in terms of this $N \to \infty$ normalization factor. Fermions enter $\tilde{\chi}$ at two-loop order, so k does not depend on m_q, since it is defined by the one-loop expression.

Thus we can make an L-dependent nonperturbative definition of the running coupling $\bar{g}$ using the value of $\tilde{\chi}(R)$ obtained from a simulation with bare coupling g_0:[2]

$$\bar{g}^2(L) \equiv \lim_{a\to 0} \frac{1}{k(r)} \hat{R}^2 \tilde{\chi}(L, a|\hat{R}), \quad \hat{R}a/L = \hat{R}/N = r = \text{fixed} \tag{2.6}$$

Note that as we shrink a, in order to hold L fixed the number of lattice sites N increases, and so must the size of the Wilson loops $\hat{R}$. Since these quantities fall off exponentially with increasing $\hat{R}$ (relative to noise) and larger lattices are significantly more expensive to simulate, this becomes a demanding computation, particularly with dynamical fermions.

To get a handle on $\bar{g}^2(L)$, we can study the scaling of the function:

$$g^2(N,r,L) \equiv \frac{1}{k(r)} \hat{R}^2 \tilde{\chi}(N, a|\hat{R})\Big|_{\hat{R}=rN} \tag{2.7}$$

On the right-hand side, the nonperturbative $\tilde{\chi}(N, a|\hat{R})$ is evaluated with system size L. Clearly if L is held fixed while N is increased, the lattice spacing is decreasing toward the continuum limit. Thus $g^2(N,r,L)$ of (2.7) defines the running coupling in a particular (nonperturbative) scheme:

$$\bar{g}^2(r|L) \equiv \lim_{N\to\infty} g^2(N,r,L). \tag{2.8}$$

The constant r is part of the renormalization scheme.

A step-scaling analysis is used to follow the running of the coupling $\bar{g}$ with the scale L. We will not actually use step-scaling in order to search for the presence of an infrared fixed point. Rather, there is a simpler, qualitative behavior that we are looking for, as we now describe.

B. Expectations

In a confining theory, $g^2(xN, r, xL) > g^2(N,r,L)$ for $x > 1$. This type of relationship means that if we hold β fixed, the measured value of $g^2(N,r,L)$ increases as N increases,

---

[2] Often below we will use the lattice coupling $\beta = 4/g_0^2$.

since $L = Na$ will increase proportionately. This leads to a behavior sketched in Fig. 1. In fact, it is easy to convince oneself that a step-scaling analysis applied using the curves in Fig. 1 will lead to a $g^2(L)$ that increases with L.

On the other hand, if there is an infrared fixed point, the ordering of curves with increasing N reverses once the bare coupling β goes past the fixed point ($\beta < \beta_*(N)$), and $g^2(xN, r, xL) < g^2(N, r, L)$ occurs for $x > 1$. Here we note that the fixed point β_* depends on N, due to lattice artifacts. Indeed, such a "backwards running" was seen at strong couplings in the SU(3) theory with sixteen fundamental flavors in the work [20, 21]. We expect something like this to also occur in the present theory at strong coupling, under the assumption that there is an infrared fixed point. Thus we expect to obtain a behavior like the one sketched in Fig. 2. Note that the curves do not all cross at the same point, which is why β_* is a function of N. Notice that there is a region of small β where the ordering of curves has clearly reversed, and that if we did a step scaling analysis in this region, the flow would be backwards.

From the vantage point of the two sketches that we have just presented, it is clear that a full blown step scaling analysis is not needed in order to detect the presence of an infrared fixed point. All that is needed is a plot of $g^2(N, r, L)$ versus β for the various N. In order to decide whether or not there is an infrared fixed point, the question that we need to answer is just this: "Which of the two figures does the plotted data look like, Fig. 1 or Fig. 2?" In fact even less is needed: it is already known from perturbation theory at weak coupling that the curves are ordered with respect to L as shown at large β. So what we need is just to show the reversal of ordering with respect to L at small β. This will be the focus of our analysis.

III. ANALYSIS

A. Smearing

We follow Bilgici et al. and apply APE smearing [24, 25] for the links that are used in the calculation of Wilson loops:

$$\begin{aligned} U_\mu(x) \;\to\; & P\{U_\mu(x) + \alpha \sum_{\nu\neq\mu} [U_\nu(x) U_\mu(x + a\hat{\nu}) U_\nu^\dagger(x + a\hat{\mu}) \\ & + U_\nu^\dagger(x - a\hat{\nu}) U_\mu(x - a\hat{\nu}) U_\nu(x - a\hat{\nu} + a\hat{\mu})]\} \end{aligned} \tag{3.1}$$

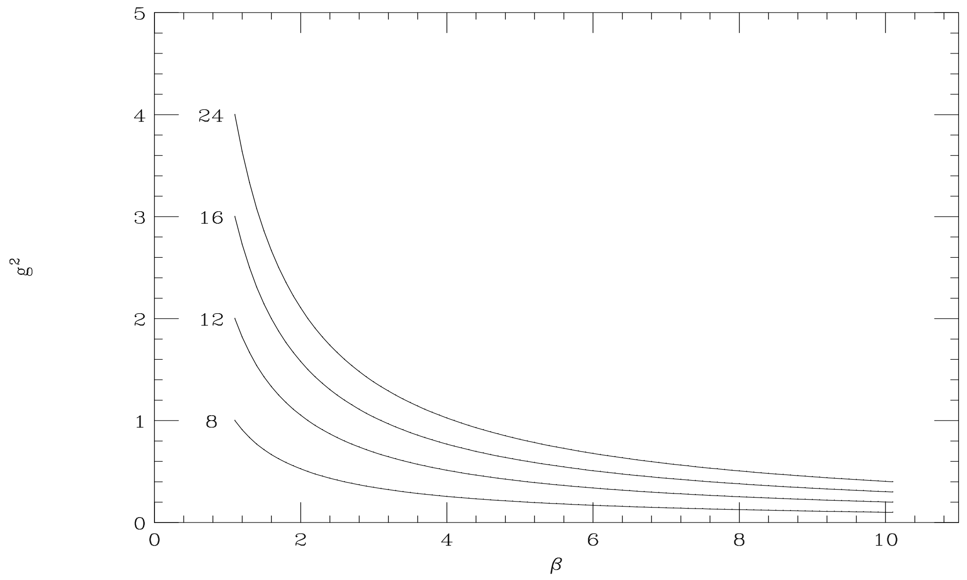

FIG. 1: Sketch of what should happen to $g^2(N, r, L)$ in a confining theory. The lines are labeled with values of N.

where P projects to a unitary matrix, which for the SU(2) group that we work with is accomplished simply by

$$A \to \frac{A}{\sqrt{\det A}} \tag{3.2}$$

for a matrix A. We take the smearing parameter to be $\alpha = 0.5$. We find that two smearing steps works well for yielding the perturbatively required increase in $g^2(N, r, L)$ with N at weak bare coupling. For this reason we use two smearing steps throughout this work.

B. Interpolation

In order to obtain a value of g^2 for $r = 1/4$ with arbitrary N, it is necessary to interpolate to values of $\hat{R}$ that are not half-integral. For this purpose Bilgici et al. introduce a quadratic hypothesis:

$$kg^2(\hat{R}) \equiv \hat{R}^2 \tilde{\chi}(\hat{R}a) \approx c_0 + c_1 \hat{R} + c_2 \hat{R}^2 \tag{3.3}$$

However, the obtained value is somewhat different if a cubic hypothesis is chosen. Furthermore, the result depends on which points are included in the fit. Here the considerations are that the smallest values of $\hat{R}$ are degraded by the smearing, and the largest values of $\hat{R}$

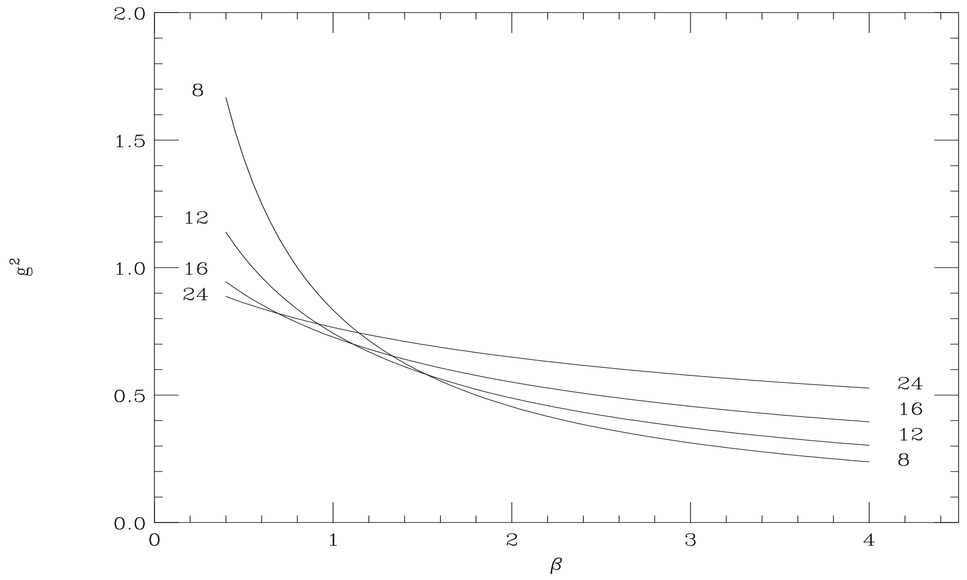

FIG. 2: Sketch of what should happen to $g^2(N, r, L)$ in a theory with an infrared fixed point. The lines are labeled with values of N.

start to reflect periodicity. We have adopted the strategy of varying all these choices and then using the variation of kg^2 as a measure of systematic error in the method. The mean value of kg^2 is used as our final estimate. Further details are given in Appendix C.

C. Results

Now that we have outlined how we obtained the values of $k(r)g^2(N, r, L)$, we proceed to discuss our results.[3] We have measured kg^2 for lattices $N = 10, 12, 16, 20, 24$ with bare coupling $\beta = 2.25$. Note that this value of β is at weaker coupling than the one where a bulk phase transition occurs, $\beta \approx 2$, as was found in [26]. It is also at a stronger coupling than the β where there was some evidence for fixed point behavior in the Schrödinger functional study [15]. Thus this point is continuously connected to the continuum limit through finite mass, but is expected to be on the strong side of the infrared fixed point. That is, we have reason to suspect backwards running for the choice $\beta = 2.25$. We have performed our

---

[3] We do not need the actual value of $k(r = 1/4)$ since it is a fixed constant independent of N. However, in Appendix B we consider an alternate definition of the running coupling where k depends on N, and in that case we do determine and divide by it.

simulations for five values of the bare mass $m_0 a$, shown in Table I. We have measured the PCAC mass $m_q a$ from the largest lattices ($N = 24$), where there is the least systematic error from finite volume. These are also given in Table I. We then extrapolate $k(r)g^2(N, r, L)$ to the $m_q = 0$ limit with quadratic and cubit fits to the data. In the case of the quadratic fit, we also consider the case where only the lightest four masses are included in the fit. The results for the measured values of kg^2 are summarized in Table II and the results of the zero mass fits are presented in Table III. The results of Table II are displayed along with the quadratic fits to all data in Fig. 3.

At large mass one sees the behavior characteristic of asymptotic freedom:

$$g^2(24) > g^2(20) > g^2(16) > g^2(12) > g^2(10). \tag{3.4}$$

In the case of the quadratic fit to all data, when we extrapolate to the chiral limit the trend reverses:

$$g^2(24) \approx g^2(20) < g^2(16) < g^2(12) \approx g^2(10). \tag{3.5}$$

Thus for this extrapolation we find backward running in the massless limit. However, in the other two extrapolations of Table III, what we see is that there is no clear pattern, but instead a rough equality:

$$g^2(24) \sim g^2(20) \sim g^2(16) \sim g^2(12) \sim g^2(10). \tag{3.6}$$

Thus what one has in this case is evidence for an absence of running.

We note that the χ^2 per degree of freedom (d.o.f.) is quite large for most of the fits. The error estimates take this into account but the implication is that the mass dependence of kg^2 is complicated and not a simple polynomial. In such a case on can question the reliability of the zero mass extrapolations. Appeal must finally be made to the results at $m_0 a = -1.18$, which shows a rough equality between the values of kg^2. We expect that this will also hold for the massless limit. In conclusion, our results seem to favor an absence of running, though there is a hint of backwards running from one of the extrapolations.

The behavior that we have observed is consistent with the existence of an infrared fixed point. We regard our results as suggestive that Minimal Walking Technicolor does not actually walk, but is instead inside the conformal window. This is supportive of the findings of Schrödinger functional studies, but now by a different method.

m_0a	m_qa
-1.000	0.448406(5)
-1.100	0.236337(4)
-1.165	0.090917(2)
-1.175	0.066873(6)
-1.180	0.054890(3)

TABLE I: PCAC mass obtained from $24^3 \times 48$ lattices.

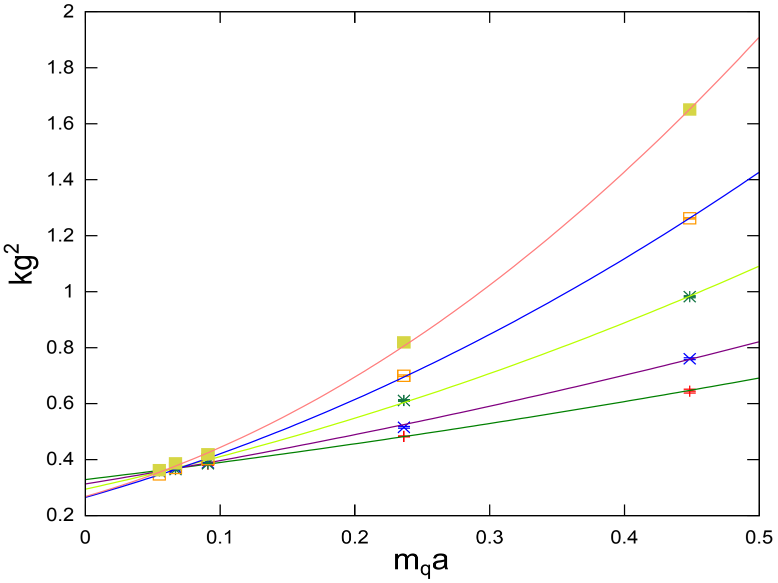

FIG. 3: Values of kg^2 for $\beta = 2.25$, $r = 1/4$. At large mass, g^2 increases with increasing N, so that the curves are ordered top to bottom, $N = 24, 20, 16, 12, 10$. However, in the massless limit, the ordering of the curves shows a trend of reversal, indicating backward running.

IV. CONCLUSIONS

We have found that the qualitative behavior of the coupling $g^2(N, r, L)$, defined through the Creutz ratio, is consistent with the existence of an infrared fixed point. We arrived at this conclusion by arguing that two different behaviors are possible, sketched in Figs. 1 and 2. We compared our data for $g^2(N, r, L)$ to these figures and find that as the fermion mass is reduced toward zero, the ordering of the points either reverses at strong bare couplings or is roughly constant, corresponding to the region where there is a crossing of curves in Fig. 2.

	$m_0a = -1.000$	$m_0a = -1.100$	$m_0a = -1.165$	$m_0a = -1.175$	$m_0a = -1.180$
$10^3 \times 20$	0.6448(67)(0)	0.4832(18)(0)	0.38394(48)(0)	0.36808(87)(0)	0.3630(10)(0)
$12^3 \times 24$	0.7604(6)(32)	0.5154(2)(32)	0.3884(2)(16)	0.37183(16)(66)	0.35661(19)(35)
$16^3 \times 32$	0.9820(10)(37)	0.6114(8)(31)	0.3954(3)(18)	0.3647(2)(13)	0.35906(20)(97)
$20^3 \times 40$	1.2621(12)(21)	0.6998(11)(28)	0.4018(3)(13)	0.3703(4)(22)	0.3474(3)(17)
$24^3 \times 48$	1.6510(15)(7)	0.8109(15)(12)	0.4192(5)(10)	0.3870(24)(7)	0.3623(8)(18)

TABLE II: Results for kg^2 for the various sizes of lattices and bare masses. The first error in kg^2 is statistical, determined by jackknife analysis of fits to the Creutz ratios as described in the text. The second error in kg^2 is systematic, obtained from varying the method of interpolation used to obtain the value at $\hat{R} = 0.25(L/a)$. This is described in more detail in Appendix blah.

	Quadratic, last 4 pts.		Quadratic, all 5 pts.		Cubic, all 5 pts.	
	kg^2	χ^2/d.o.f.	kg^2	χ^2/d.o.f.	kg^2	χ^2/d.o.f.
$10^3 \times 20$	0.3312(49)	2.52	0.3288(26)	1.75	0.3321(58)	2.44
$12^3 \times 24$	0.297(17)	23.6	0.3130(95)	25.7	0.291(20)	21.3
$16^3 \times 32$	0.319(20)	12.7	0.295(11)	19.0	0.327(23)	11.4
$20^3 \times 40$	0.284(15)	5.04	0.2651(85)	7.88	0.288(18)	5.36
$24^3 \times 48$	0.313(18)	7.12	0.268(14)	29.5	0.321(22)	7.81

TABLE III: Results for the zero mass extrapolation of kg^2 for the various sizes of lattices.

While it would be disappointing from a phenomenological point of view if Minimal Walking Technicolor is actually conformal in the infrared, it is nevertheless significant that by more than one method lattice field theory technique evidence has been obtained for the existence of an infrared fixed point. Furthermore, conformal theories are inherently interesting and more detailed studies of the present gauge theory are worth pursuing on the lattice.

Two refinements to the present study could be performed, which would hopefully yield firmer conclusions. First, smaller PCAC masses should be simulated so that a stronger case for what happens in the chiral limit can be made. Second, larger volumes such as $N = 32$ should be simulated, so that the trends with respect to N can be amplified, hopefully clarifying whether or not backwards running actually occurs. We are presently pursuing these two improvements and will report on them in the future.

Acknowledgements

This research was supported by the Dept. of Energy, Office of Science, Office of High Energy Physics, Grant No. DE-FG02-08ER41575. EW was also supported by the summer 2010 REU program in physics at RPI, funded by the National Science Foundation award DMR 0850934 REU site at Rensselaer. We gratefully acknowledge the sustained use of RPI computing resources over the course of a year, both the on-campus SUR IBM BlueGene/L rack, as well as continuous access to 1-4 racks of the sixteen IBM BlueGene/L's situated at the Computational Center for Nanotechnology Innovation.

Appendix A: Computing methods and resources

Simulations are performed using Hybrid Monte Carlo [27], which is the standard method for dynamical fermions. Our lattice action is Wilson fermions and a plaquette gauge action. Our sampling of configurations is separated by five molecular dynamics time units, and we use 1000 samples on all lattices excepting $N = 24$, $m_0 a = -1.175, -1.180$ where we used 700 samples in each case. (This was the most expensive part of the computation.) The parallel simulation and analysis code that we use is a modification of the Columbia Physics System, in order to incorporate SU(2) gauge group and adjoint fermions. It was originally developed for the study of $\mathcal{N} = 1$ super-Yang-Mills [28], but has recently been used for the Minimal Walking Technicolor gauge theory [26, 29]. All simulations were performed on IBM BlueGene/L computers at RPI, both an on-campus rack and one to four of the sixteen racks at the Computational Center for Nanotechnology Innovation. Our larger lattices were simulated using an entire rack, while our smaller lattices used smaller partitions. Suffice it to say, significant computing resources were dedicated to this project over a period of about one year. We estimate that 7 million BlueGene/L core hours were expended for the research summarized in this article. Smearing to obtain the Wilson loops that are used for our Creutz ratios was also performed in parallel, though this analysis step consisted of only a small fraction of our computing time. Finally, we computed the correlation functions necessary for obtaining the PCAC mass using the parallel resources, which again only consumed a small fraction of the computing time.

The remainder of the numerical analysis for this project was performed on a single workstation. This involved averaging the data with a jackknife analysis of fits in order to obtain errors in our values of kg^2. Similarly, the final steps of the analysis to obtain PCAC masses were performed with jackknife error estimation.

Appendix B: Alternative definition

Since there is no unique definition of the running coupling at finite N, one could also use the value of k at finite N. That is,

$$g^2(N,r,L) = \frac{1}{k(r,N)} \hat{R}^2 \tilde{\chi}(L,a|\hat{R}) \tag{B1}$$

For this, since we choose $r = 1/4$ it is necessary to interpolate $k(r,N)$ between values of r that are allowed for a given N (we use a quadratic fit at fixed N). For the determination of k, we use the results of [30], which leads to the following formulae. First their is the contribution of Wilson loops which do not have links in the temporal direction:

$$c_1^{(0)}(I,J) = \frac{N_c^2-1}{N_c^2} \left\{ \frac{1}{4V} \sum_{p\neq 0} \frac{1}{|P(p)|^2} \left(|e^{ip_1 I} - 1|^2 \left| \sum_{k=0}^{J-1} e^{ikp_2} \right|^2 + (I \leftrightarrow J, 1 \leftrightarrow 2) \right) \right\} \tag{B2}$$

N_c is the number of colors; $N_c = 2$ in our case. The quantities $|P(p)|^2$ and V are defined below. A similar formula holds for the Wilson loops with two links in the temporal direction:

$$c_1^{(2)}(I,J) = \frac{N_c^2-1}{N_c^2} \left\{ \frac{1}{4V} \sum_{p\neq 0} \frac{1}{|P(p)|^2} \left(|e^{ip_0 I} - 1|^2 \left| \sum_{k=0}^{J-1} e^{ikp_1} \right|^2 + (I \leftrightarrow J, 0 \leftrightarrow 1) \right) \right\} \tag{B3}$$

In these expressions, the momenta take the following values, given that there are N sites in the spatial directions and $2N$ sites in the temporal direction ($i = 1,2,3$):

$$p_0 = n_0\pi/N, \quad p_i = 2n_i\pi/N, \quad n_0 = 0,\ldots,2N-1, \quad n_i = 0,\ldots,N-1 \tag{B4}$$

Also, we have the definitions:

$$P_\mu(p) = e^{ip_\mu} - 1, \quad |P(p)|^2 = \sum_\mu |P_\mu(p)|^2, \quad V = 2N^4 \tag{B5}$$

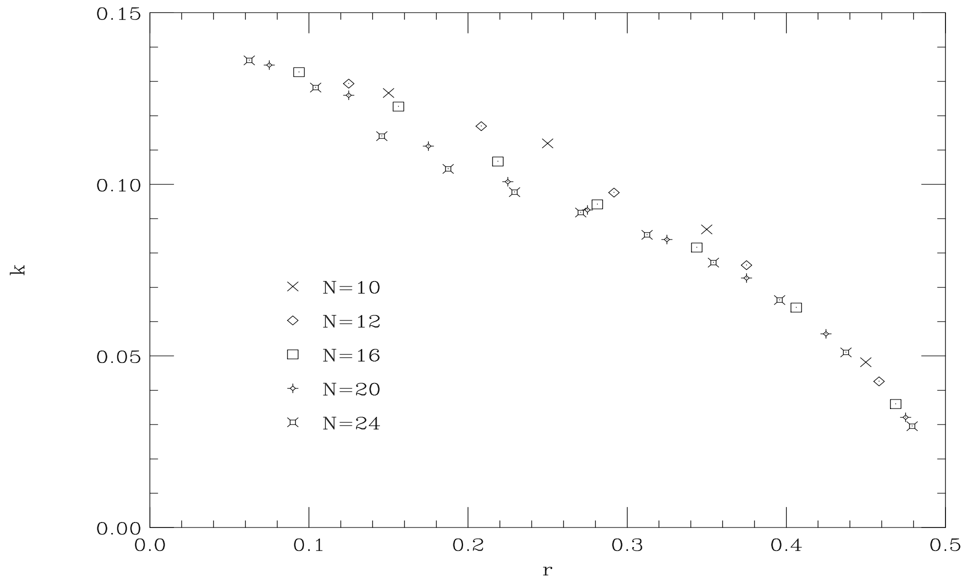

FIG. 4: $k(r,N)$ for the lattices that we study.

The zero-model contribution must also be included:

$$c_1^{(0)} = c_1(p=0) + c_1^{(0)}, \quad c_1^{(2)} = c_1(p=0) + c_1^{(2)}, \quad c_1(p=0;I,J) = \frac{N_c^2-1}{12N_c^2}\frac{(IJ)^2}{V} \tag{B6}$$

Finally, the Creutz ratio at this order of lattice perturbation theory is:

$$\begin{aligned}\chi(I,I)_{\text{1-loop}} \;=\; & g_0^2 N_c \frac{1}{2}[c_1^{(2)}(I,I) + c_1^{(0)}(I,I) + c_1^{(2)}(I-1,I-1) \\ & + c_1^{(0)}(I-1,I-1) - c_1^{(2)}(I,I-1) - c_1^{(2)}(I-1,I) - 2c_1^{(0)}(I,I-1)]\end{aligned} \tag{B7}$$

where g_0 is the bare coupling. From this we extract k at finite N:

$$k(r,N) = \frac{1}{g_0^2}\left(I - \frac{1}{2}\right)^2 \chi(I,I)_{\text{1-loop}}, \quad r = \left(I - \frac{1}{2}\right)/N. \tag{B8}$$

In Fig. 4 we show $k(r,N)$ for the lattices that we study, taking the range $I = 2, \ldots, N/2$. We note that our values of $k(r,N)$ are in agreement with those of [18, 19], once the difference in color factors $(N_c^2-1)/N_c$ is taken into account (they have $N_c = 3$).

We have calculated g^2 by this alternate approach, for the case of quadratic extrapolation fitted to all data points, and the results are summarized in Table IV. The behavior of decreasing coupling with increasing N seems to persist with this modified definition of the running coupling.

$k(1/4,N)$	g^2
0.111952	2.937(23)
0.108871	2.875(87)
0.103207	2.85(10)
0.0995411	2.663(85)
0.0971746	2.76(14)

TABLE IV: g^2 calculated by the method where different values of k are used for each N.

Lattice	I_{start}	I_{end}	Fit
$10^3 \times 20$	2	5	2
$12^3 \times 24$	3	7,8	2,3
$16^3 \times 32$	3,4	7,8	2,3
$20^3 \times 40$	3,4,5	7,8	2,3
$24^3 \times 48$	4,5	9,10	2,3

TABLE V: Choices of parameters that were varied for the fit that is used in the interpolation to obtain $kg^2(\hat{R} = N/4)$.

Appendix C: Systematic error estimates

As described in the main text, an interpolation of $kg^2(\hat{R})$ to the value $\hat{R} = N/4$ is required, since $\chi(I,I)$ only takes values at integer I and $\hat{R} = I - \frac{1}{2}$. This allows for various choices for the range of the fit, $I_{\text{start}}, \ldots, I_{\text{end}}$. One can also choose to fit with a quadratic (Fit=2) or cubic (Fit=3) hypothesis for $kg^2(\hat{R})$, as a function of $\hat{R}$. We have varied these options, constrained by what is possible on the various lattices, and have used the standard deviation of the interpolated values as a measure of systematic error. Because of smearing it is important that we choose I_{start} as large as possible on a given lattice. In Table V we present the various parameter choices that were used. The mean of the interpolated values is used as our estimate for kg^2.

---

[1] Leonard Susskind. Dynamics of Spontaneous Symmetry Breaking in the Weinberg- Salam Theory. *Phys. Rev.*, D20:2619–2625, 1979.

[2] Steven Weinberg. Implications of Dynamical Symmetry Breaking: An Addendum. *Phys. Rev.*, D19:1277–1280, 1979.

[3] Bob Holdom. Raising the Sideways Scale. *Phys. Rev.*, D24:1441, 1981.

[4] Bob Holdom. Techniodor. *Phys. Lett.*, B150:301, 1985.

[5] Koichi Yamawaki, Masako Bando, and Ken-iti Matumoto. Scale Invariant Technicolor Model and a Technidilaton. *Phys. Rev. Lett.*, 56:1335, 1986.

[6] M. Bando, K. Matumoto, and K. Yamawaki. Technidilaton. *Phys. Lett.*, B178:308, 1986.

[7] Thomas W. Appelquist, Dimitra Karabali, and L. C. R. Wijewardhana. Chiral Hierarchies and the Flavor Changing Neutral Current Problem in Technicolor. *Phys. Rev. Lett.*, 57:957, 1986.

[8] Thomas Appelquist and L. C. R. Wijewardhana. Chiral Hierarchies and Chiral Perturbations in Technicolor. *Phys. Rev.*, D35:774, 1987.

[9] Thomas Appelquist and L. C. R. Wijewardhana. Chiral Hierarchies from Slowly Running Couplings in Technicolor Theories. *Phys. Rev.*, D36:568, 1987.

[10] Estia Eichten and Kenneth D. Lane. Dynamical Breaking of Weak Interaction Symmetries. *Phys. Lett.*, B90:125–130, 1980.

[11] Kenneth D. Lane and Estia Eichten. Two Scale Technicolor. *Phys. Lett.*, B222:274, 1989.

[12] Francesco Sannino and Kimmo Tuominen. Techniorientifold. *Phys. Rev.*, D71:051901, 2005.

[13] T. Appelquist, G. T. Fleming and E. Neil. Lattice Study of the Conformal Window in QCD-like Theories. *Phys. Rev. Lett.*, 100:171607, 2008.

[14] Yigal Shamir, Benjamin Svetitsky, and Thomas DeGrand. Zero of the discrete beta function in SU(3) lattice gauge theory with color sextet fermions. *Phys. Rev.*, D78:031502, 2008.

[15] Ari J. Hietanen, Kari Rummukainen, and Kimmo Tuominen. Evolution of the coupling constant in SU(2) lattice gauge theory with two adjoint fermions. *Phys. Rev.*, D80:094504, 2009.

[16] Francis Bursa, Luigi Del Debbio, Liam Keegan, Claudio Pica, and Thomas Pickup. Running of the coupling and quark mass in SU(2) with two adjoint fermions. *PoS*, LAT2009:056, 2009.

[17] Thomas DeGrand, Yigal Shamir, and Benjamin Svetitsky. Infrared fixed point in SU(2) gauge

theory with adjoint fermions. 2011.

[18] Erek Bilgici et al. A New Method of Calculating the Running Coupling Constant. *PoS*, LATTICE2008:247, 2008.

[19] Erek Bilgici et al. A new scheme for the running coupling constant in gauge theories using Wilson loops. *Phys. Rev.*, D80:034507, 2009.

[20] Zoltan Fodor, Kieran Holland, Julius Kuti, Daniel Nogradi, and Chris Schroeder. Calculating the running coupling in strong electroweak models. *PoS*, LAT2009:058, 2009.

[21] Zoltan Fodor, Kieran Holland, Julius Kuti, Daniel Nogradi, and Chris Schroeder. Nearly conformal gauge theories in finite volume. *Phys. Lett.*, B681:353–361, 2009.

[22] Hiroshi Ohki, Tatsumi Aoyama, Etsuko Itou, Masafumi Kurachi, C.-J.David Lin, et al. Study of the scaling properties in SU(2) gauge theory with eight flavors. *PoS*, LATTICE2010:066, 2010.

[23] Michael Creutz. Asymptotic Freedom Scales. *Phys. Rev. Lett.*, 45:313, 1980.

[24] M. Albanese et al. Glueball Masses and String Tension in Lattice QCD. *Phys. Lett.*, B192:163–169, 1987.

[25] M. Teper. An Improved Method for Lattice Glueball Calculations. *Phys. Lett.*, B183:345, 1987.

[26] Simon Catterall, Joel Giedt, Francesco Sannino, and Joe Schneible. Phase diagram of $SU(2)$ with 2 flavors of dynamical adjoint quarks. *JHEP*, 11:009, 2008.

[27] S. Duane, A. D. Kennedy, B. J. Pendleton, and D. Roweth. Hybrid Monte Carlo. *Phys. Lett.*, B195:216–222, 1987.

[28] Joel Giedt, Richard Brower, Simon Catterall, George T. Fleming, and Pavlos Vranas. Lattice super-Yang-Mills using domain wall fermions in the chiral limit. *Phys. Rev.*, D79:025015, 2009.

[29] S. Catterall, J. Giedt, F. Sannino and J. Schneible. Probes of nearly conformal behavior in lattice simulations of minimal walking technicolor. 2009 [arXiv:0910.4387].

[30] A. Coste, Antonio Gonzalez-Arroyo, J. Jurkiewicz, and C. P. Korthals Altes. ZERO MOMENTUM CONTRIBUTION TO WILSON LOOPS IN PERIODIC BOXES. *Nucl. Phys.*, B262:67, 1985.